QUANTUM THEORY OF THREE-DIMENSIONAL SUPERRESOLUTION USING ROTATING-PSF IMAGERY

Sudhakar Prasad and Zhixian Yu
Department of Physics and Astronomy, University of New Mexico, Albuquerque, NM 87131

The inverse of the quantum Fisher information (QFI) matrix (and extensions thereof) provides the ultimate lower bound on the variance of any *unbiased* estimation of a parameter from statistical data, whether of intrinsically quantum mechanical or classical character. We calculate the QFI for Poisson-shot-noise-limited imagery using the rotating PSF that can localize and resolve point sources fully in all three dimensions. We also propose an experimental approach based on the use of computer generated hologram and projective measurements to realize the QFI-limited variance for the problem of super-resolving a closely spaced pair of point sources at a highly reduced photon cost. The paper presents a preliminary analysis of quantum-limited three-dimensional (3D) pair optical super-resolution (OSR) problem with potential applications to astronomical imaging and 3D space-debris localization.

1 Introduction

OSR is concerned with the ability of an imager to separate a pair of point sources that are spaced closer than the angular Rayleigh resolution limit, of order λ/D, when using light of mean wavelength λ and a telescope primary of diameter D. The fact that this is essentially a visual limit, however, rather than a fundamental law, one that can be overcome in practical instruments at sufficiently large photon fluxes is now widely accepted [1–6].

Statistical estimation theory provides a fundamental bound on how small a separation between the source pair can be resolved. This lower bound, based on the statistical model of the data, is given by the inverse of Fisher information (FI) [7, 8], which is a first-order differential sensitivity measure, and thus is only determined by the nature and level of noise in the data vector, $\mathbf{X}$. Classically, FI with respect to a set of n parameters, $\Theta \stackrel{\text{def}}{=} \{\theta_1, \ldots, \theta_n\}$, is defined as an $n \times n$ matrix, $\mathbf{J}$, of elements

$$J_{\mu\nu} = \mathbb{E}\left(\frac{\partial \ln P(\bar{X}|\Theta)}{\partial \theta_\mu}\frac{\partial \ln P(\bar{X}|\Theta)}{\partial \theta_\nu}\right), \tag{1}$$

where $P(\bar{X}|\Theta)$ denotes the probability distribution function (PDF) of the data $\bar{X}$, given the set Θ of paramater values. The diagonal elements of the inverse of $\mathbf{J}$ yield lower bounds on *any* unbiased estimation of the n parameters. We call $\mathbf{J}$ classical FI (CFI) as it is based on classical statistical data that have a non-negative probability distribution.

There is a quantum version of the FI [9] that only depends on the system state, described by its density operator, $\hat{\rho}(\Theta)$, not on the nature of the measurements made on it as described by a positive operator valued measure (POVM) comprised of positive operators that add up to the identity operator. The quantum FI (QFI) matrix elements with respect to the parameter set Θ are defined as

$$H_{ij} = \mathrm{Tr}\,(\hat{\rho}\hat{L}_i\hat{L}_j), \tag{2}$$

where $\hat{L}_i$ is the symmetric logarithmic derivative of $\hat{\rho}$ with respect to the parameter θ_i that is defined by the relation

$$\frac{\partial\hat{\rho}}{\partial\theta_i} = \frac{1}{2}\left(\hat{L}_i\hat{\rho} + \hat{\rho}\hat{L}_i\right). \tag{3}$$

The QFI provides the ultimate lower bound on the variance of an unbiased estimation of the parameters superseding that provided by the CFI, as the former is a supremum over all possible measurements, including *all* classical ones and those that are not over mutually exclusive outcomes, *i.e.*,

$$\sigma_i^2 \geq \mathbf{J}_{ii}^{-1} \geq \mathbf{H}_{ii}^{-1}. \tag{4}$$

For the problem of pair OSR being considered here, we shall apply both QFI and CFI to a single-photon quantum state of light emitted by a pair of closely spaced point sources, and show that the QFI for estimating their 3D separation is in fact strictly a constant even in the limit of vanishing separation. This is quite unlike the CFI for image-based measurement of the pair separation, which typically tends to zero in this limit quadratically in the separation coordinates. Thus, QFI if achievable can qualitatively reduce the photon budget needed to perform pair OSR in the sub-Rayleigh-separation regime. A recent theoretical paper by Tsang *et al.* [10] and a subsequent experimental study

by another group [11] quickly thereafter confirmed that QFI for pair OSR is indeed achievable via projective measurements, which are rather analogous to compressed sensing (CS). The present paper advances a preliminary analysis of the 3D pair OSR problem based on the projective measurement approach, extending thus the previous work to 3D OSR.

Rotating PSF imagery, proposed by Prasad [12], furnishes a practical approach to perform 3D source localization using a spiral phase mask that generates a combination of Bessel vortex beams. For a special annular design of the mask, with the spiral-phase winding number in successive annuli changing by a fixed quantum number, this Bessel-beam combination can yield an off-center image that rotates with changing object-space or image-space distance without diffractively degrading over a large axial depth. For microscopy this depth range can be 10-20 microns wide at optical wavelengths, a range beyond which the point-source image, the so called point-spread function (PSF), breaks apart due to diffraction. In telescopic imaging, this range can be tens of meters at kilometric distances, over which such a rotating PSF imager to perform snapshot 3D localization of unresolved and small sources. This would allow to localize and track small space debris when sufficiently illuminated and reflecting at distances of hundreds of meters to a few kilometers using asset-mounted cameras equipped with such phase masks in the snapshot mode.

In this paper we evaluate the various FI metrics for the rotating-PSF imagery. We will first calculate the 3×3 QFI matrix for 3D OSR with respect to (w.r.t.) the pair semi-separation vector, $\Delta\mathbf{r}$, which turns out to be a constant, diagonal matrix independent of $\Delta\mathbf{r}$. We will then calculate both image-data-based CFI and projective CFI matrices, the latter based on the notion of spatial demultiplexing (SPADE) of the single-photon state emitted by an incoherent source pair into specially chosen single-photon basis states that tend to localize the photon in all three dimensions. For an orthonormal basis, these projections yield the corresponding probabilities of finding the photon in these states, which in turn can be used to determine the classical FI in this projection basis, rather than the pixel basis in which image based data live. The CFI for the projection and pixel bases then yield, respectively, the CFI matrices for projective and image-based data w.r.t. the separation vector. Finally, we shall consider projective-measurement protocols in which the smallest possible variance of estimating the three separation coordinates as given by the inverse of the QFI matrix can in fact be achieved in the important limit of vanishing separation. Pixel based image data can never achieve such estimation variances in this limit, as we will also show.

2 Quantum Fisher Information for 3D Pair Separation

When an incoherent pair of equally bright point sources that are at the 3D locations, $\pm\Delta\mathbf{r}$, emits a photon that is subsequently transmitted through an imager, it has the density operator,

$$\hat{\rho} = \frac{1}{2}\left(|K_+\rangle\langle K_+| + |K_-\rangle\langle K_-|\right), \tag{5}$$

in which $|K_\pm\rangle$ are pure one-photon states corresponding to the two sources. Their coordinate representations, $\langle\mathbf{s}|K_\pm\rangle$, in the image plane are simply the amplitude point-spread functions (PSFs), $K(\mathbf{s};\pm\Delta\mathbf{r})$, corresponding to the two displaced sources. If the imaging aperture imposes a complex amplitude function, $\eta(\mathbf{u})\exp[i\Psi(\mathbf{u})]$, on the incoming imaging wave, then we may write $K(\mathbf{s};\pm\Delta\mathbf{r})$ as the integral,

$$\begin{aligned} K(\mathbf{s};\pm\Delta\mathbf{r}) =& \langle\mathbf{s}|K_\pm\rangle \\ =& \mathcal{N}\int d^2u P(u)\,\eta(\mathbf{u})\exp[i\Psi(\mathbf{u}) \pm i\pi l_z u^2]\exp[2\pi i\mathbf{u}\cdot(\mathbf{s}\mp\boldsymbol{l}_\perp)]. \end{aligned} \tag{6}$$

The dimensionless transverse vector, $\boldsymbol{l}_\perp$, and axial coordinate, l_z, in expression (6) are related to the physical source displacement, $\Delta\mathbf{r} = (\Delta x, \Delta y, \Delta z)$, from the origin by the following scaling:

$$\boldsymbol{l}_\perp = (l_x, l_y) \text{ with } (l_x, l_y) = \frac{1}{\lambda/\mathrm{NA}}(\Delta x, \Delta y);\ l_z = \frac{\Delta z}{\lambda/\mathrm{NA}^2}, \tag{7}$$

with $\mathrm{NA} = R/z_O$ being the numerical aperture (NA) of the imager with aperture radius R and z_O the source distance from the aperture. The indicator function, $P(u)$, is 1 inside the aperture, $0 \le u < 1$, and 0 outside, with $\mathbf{u}$ being the aperture position vector normalized by dividing it by R. We express the image-plane position vector in dimensionless units by dividing it by the Airy-radius parameter, λ/NA, which we denote as $\mathbf{s}$. To arrive at the simplified expression (6) for the amplitude PSF, we have further chosen the magnification to be unity, but it is easy to multiply $\mathbf{s}$ by the ratio

of source and image plane distances from the aperture, namely $-z_O/z_I$, on the right-hand side to account for non-unit magnification.

These wave functions are normalized by choosing the coefficient $\mathcal{N}$ so that $\langle K_\pm\rangle\langle K_\pm\rangle = 1$, *i.e.*, their squared moduli, namely the corresponding incoherent PSFs, integrate to 1:

$$\langle K_\pm\rangle\langle K_\pm\rangle = \int d^2s|K(\mathbf{s};\pm\Delta\mathbf{r})|^2 = 1. \tag{8}$$

Since the density operator (5) is a rank-two operator, it has only two non-zero eigenvalues, $d_\pm$, which along with the corresponding eigenstates, $|e_\pm\rangle$, are easily calculated and given by the relations,

$$d_\pm = \frac{1\pm|D|}{2};\;\; |e_\pm\rangle = \frac{1}{\sqrt{2(1\pm|D|)}}\left(|K_+\rangle \pm \frac{D}{|D|}|K_-\rangle\right), \tag{9}$$

with D defined as the inner product,

$$D = \langle K_-|K_+\rangle, \tag{10}$$

which is the overlap integral, in coordinate space, between the amplitude PSFs corresponding to the two point sources.

The remaining eigenstates are all degenerate with eigenvalue 0. The completeness of all the eigenstates of $\hat{\rho}$, guaranteed by its hermiticity, may be used to express the $\mu\nu$ element of the QFI defined by Eqs. (2) and (3) in terms of $d_\pm$ and eigenstates $|e_\pm\rangle$ as

$$\begin{aligned} H_{\mu\nu} = &\sum_{j,k=\pm} d_j\left[\left(\frac{2}{d_j+d_k}\right)^2 - \left(\frac{2}{d_j}\right)^2\right]\langle e_j|\frac{\partial\hat{\rho}}{\partial\theta_\mu}|e_k\rangle\langle e_k|\frac{\partial\hat{\rho}}{\partial\theta_\nu}|e_j\rangle \\ &+\sum_{j=\pm} d_j\left(\frac{2}{d_j}\right)^2\langle e_j|\frac{\partial\hat{\rho}}{\partial\theta_\mu}\frac{\partial\hat{\rho}}{\partial\theta_\nu}|e_j\rangle. \end{aligned} \tag{11}$$

The derivation of result (11) will appear in the paper [13].

The QFI matrix elements, $H_{\mu\nu}$, may be calculated from the form of the eigenvalues and eigenvectors given by (9), the form (5) of the density operator, and the form (6) of the amplitude PSFs. The calculations are quite involved and tedious, but a number of simplifications result from the inversion symmetry of the circular aperture we assume in the problem. When they are all properly included, the following constant, diagonal form of QFI with respect to the three separation coordinate parameters, l_x, l_y, l_z, is obtained:

$$H(l_x,l_y,l_z) = \begin{pmatrix} 4\pi^2 & 0 & 0 \\ 0 & 4\pi^2 & 0 \\ 0 & 0 & \dfrac{\pi^2}{3} \end{pmatrix}. \tag{12}$$

All FI calculations of this paper are w.r.t. the three dimensionless source-separation parameters, l_x, l_y, l_z. The minimum estimation variances, in physical units, are given by inverting our FI matrices and then multiplying their diagonal elements by the squares of the scales introduced in (7), namely $(\lambda/\mathrm{NA})^2$ for the transverse coordinates and $(\lambda/\mathrm{NA}^2)^2$ for the axial coordinate of the separation vector.

Pair OSR vs. Source Localization As we see from Eq. (12), QFI is rather surprisingly independent of the three parameters. In other words, even when the separation tends to 0, QFI does not decay to zero, unlike FI based on image data as we shall see in the next section. This constancy of QFI traces back to the very nature of source-separation information about the source pair at the most fundamental level of individual photon measurements, namely that it is the ability to localize individual photons that ulimately bounds the information about the separation of a pair of point sources. The problem of source separation in effect reduces to the problem of photon, or source, localization when considered at its most fundamental level. We have confirmed this conjecture by calculating the QFI for the localization of a single point source and showing that the two QFIs are in fact identical. Details of these calculations will be presented in Ref. [13].

3 Two Different Pair OSR Protocols and Corresponding CFI

We now compare the FI for two different protocols to estimate the pair-separation parameters, l_x, l_y, l_z, namely image-data-based estimation under Poisson statistics of counts, as would be appropriate for EM-CCD detectors, and projective SPADE measurements.

3.1 Poisson Image Data and CFI

The image data are assumed to follow Poisson statistics around the mean pixel values given by multiplying the pixel area, ΔA, by the mean incoherent image data recorded by the image sensor at its pth pixel centered at $\mathbf{s}_p$, which in view of (5) and (6) has the form

$$\begin{aligned} N_p =& N\Delta A\langle \mathbf{s}_p|\hat{\rho}|\mathbf{s}_p\rangle \\ =& \frac{N\Delta A}{2}\left[|K(\mathbf{s};\boldsymbol{l}_\perp, l_z)|^2 + |K(\mathbf{s};-\boldsymbol{l}_\perp;-l_z)|^2\right], \end{aligned} \tag{13}$$

where N is the mean photon number that is captured by the imager viewing the source pair. We have also implictly transformed the semi-separation vector $\Delta\mathbf{r}$ to its normalized form, $(\boldsymbol{l}_\perp, l_z)$. The partial derivative of the log-likelihood function (LLF) of the counts, $\{p_1, p_2, \ldots\}$, with respect to a parameter, θ_μ, on which the mean counts, $\{N_1, N_2, \ldots\}$, are functionally dependent is just the pixel sum,

$$\frac{\partial \ln P}{\partial \theta_\mu} = \sum_p \left(\frac{n_p}{N_p} - 1\right)\frac{\partial N_p}{\partial \theta_\mu}. \tag{14}$$

Multiplying Eq. (14) by a similar expression for the partial derivative of the LLF w.r.t. θ_μ and taking the expectation of the product over the Poisson probability distribution, we obatin the following matrix element for the CFI as defined in Eq. (1):

$$J_{\mu\nu} = \sum_p \frac{1}{N_p}\frac{\partial N_p}{\partial \theta_\mu}\frac{\partial N_p}{\partial \theta_\nu}, \tag{15}$$

in which we used the Poisson variance law, $\mathbb{E}[(n_p - N_p)(n_q - N_q)] = \delta_{pq}N_p$, valid for statistically independent pixel counts. Here $\mathbb{E}$ denotes statistical expectation.

The above matrix elements of the CFI may be evaluated numerically as a function of the three coordinates, l_x, l_y, l_z, of normalized separation vector. An order-of-magnitude calculation based on the expression (13) for N_p for small separations, $l_x, l_y, l_z << 1$, follows on expanding N_p in powers of l_x, l_y, l_z, and keeping only the lowest-order dependence on them. It is clear that the lowest-order dependence of the symmetric sum in (13) is quadratic in these parameters, so its partial derivative relative to these parameters is then linear in them, yielding thus, on substitution in (15), a 3×3 CFI matrix whose $\mu\nu$ element scales as N times $l_\mu l_\nu$ in the separation parameters to be estimated. The inverse of this matrix then has diagonal elements, which are the lowest possible unbiased estimation variances, with an inverse square law dependence on these parameters,

$$\mathbf{J}^{-1}_{\mu\mu} \sim \frac{1}{Nl_\mu^2}, \;\; \mu = x, y, z, \tag{16}$$

which must be smaller than the squared separation parameter, l_μ^2, implying thus a quartic power-law dependence of the minimum photon number, $N_{\min} \sim l_\mu^{-4}$, needed to resolve a squared normalized pair-separation of order l_μ^2 accurately. Such scalings are quite typical of all estimations that utilize image-based data.

3.2 Projective Measurements and CFI

Equation (5) describes the density operator of the state of a single light photon emitted by an incoherent pair of point sources. Such sources could be thermal sources like stars from which light emission carries only a small mean photon number per mode. As a result, the statistics of the photon count from such sources over long measurement times are in effect Poissonian. The question we ask is the following: What is the probability that the photon will be detected in one of a complete orthonormal basis of states, $\{|K_{nm}\rangle \mid m, n = -\infty, \ldots, \infty\}$?

3.2.1 Rotating PSF and Related Orthonormal Basis

A particularly useful orthonormal basis of states is that inspired by the spiral phase mask (SPM) that we have previously used to generate an off-axis PSF that rotates at a constant rate with changing axial distance of the point source with respect to the plane of Gaussian focus. The rotating PSF has the following amplitude in previously introduced normalized variables:

$$\begin{aligned} K_0(\mathbf{s};\boldsymbol{l}_\perp,l_z) =& \langle \mathbf{s}|K_0;\boldsymbol{l}_\perp,l_z\rangle \\ =& \frac{1}{\sqrt{\pi}}\int d^2u\, P(u)\, \exp\left[-i2\pi\mathbf{u}\cdot(\mathbf{s}-\boldsymbol{l}_\perp+i\Psi_0(\mathbf{u})-i\pi l_z u^2\right]. \end{aligned} \tag{17}$$

Note that the incoherent PSF, $|K_0(\mathbf{s};\boldsymbol{l}_\perp,l_z)|^2$, is properly normalized in the sense that it integrates to unity over the image plane. The phase mask, $\Psi_0(\mathbf{u})$, is comprised of L annular zones, each causing an optical vortex phase of quantum number that increases by a fixed integer step from one zone to the next. For simplicity, we choose this step to be unity and thus the aperture phase mask to be of the specific form,

$$\Psi_0(\mathbf{u}) = \left\{ n\phi_u,\ \sqrt{(n-1)/L} < u < \sqrt{n/L}\ \middle|\ n=1,\ldots,L \right\}. \tag{18}$$

For this phase profile, one may show that the incoherent PSF, $|K_0(\mathbf{s};\boldsymbol{l}_\perp,l_z)|^2$ has a fairly compact support that rotates by a whole turn without much diffractive spreading over the range $(-L,L)$ of values for the axial defocus parameter, l_z. The coordinates of the center and the angle of rotation contain complete information about the 3D location of the point source.

A complete basis of orthonormal states that derives from the state (17) is the set, $\{|K_{nm}\rangle \mid n,m=-\infty,\ldots,\infty\}$, in which the state $|K_{nm}\rangle$ is defined by its image-plane representation as

$$\langle \mathbf{s}|K_{nm}\rangle = \frac{1}{\sqrt{\pi}}\int d^2u\, P(u)\, \exp\left[-i2\pi\mathbf{u}\cdot\mathbf{s}+i\Psi_n(\mathbf{u})-i2\pi m u^2\right], \tag{19}$$

with $\Psi_n(\mathbf{u})$ defined as

$$\Psi_n(\mathbf{u}) = \Psi_0(\mathbf{u}) + n\phi_u. \tag{20}$$

These states can be shown to be orthonormal and complete over the imager aperture.

We now consider making projective measurements of the single-photon state, $\hat{\rho}$, given by Eq. (5), in this basis. The probability of detecting the $|K_{nm}\rangle$ state is simply the diagonal element,

$$\begin{aligned} P_{nm} =& \langle K_{nm}|\hat{\rho}|K_{nm}\rangle \\ =& \frac{1}{2}\left(P_{nm}^{(+)}+P_{nm}^{(-)}\right), \end{aligned} \tag{21}$$

in which the two probabilities $P_{nm}^{(\pm)}$ refer to the source of the photon being the emitter at $\pm(\boldsymbol{l}_\perp,l_z)$. The latter may be evaluated as

$$P_{nm}^{(\pm)} = \left| \int_0^1 dx\, J_n\left(2\pi|\boldsymbol{l}_\perp|\sqrt{x}\right) \exp[i2\pi(m\mp l_z/2)x] \right|^2, \tag{22}$$

which shows that these probabilities do not depend on the orientation of the transverse pair separation vector, but only on its magnitude. The set of probabilities, $\{P_{nm} \mid n,m=-\infty,\ldots,\infty\}$, yields a 2×2 CFI matrix w.r.t. the transverse and axial separation parameters, $|\boldsymbol{l}_\perp|$ and l_z, which may be numerically evaluated.

A different basis, $\{|A_{nm}\rangle \mid n,m=-\infty,\ldots,\infty\}$, which is comprised of linear combinations of the $|K_{nm}\rangle$ states, namely

$$\begin{aligned} |A_{\pm n,+m}\rangle =& \frac{1}{2}[(|K_{n,m}\rangle \pm |K_{-n,m}\rangle) + (|K_{n,-m}\rangle \pm |K_{-n,-m}\rangle)]; \\ |A_{\pm n,-m}\rangle =& \frac{1}{2}[(|K_{n,m}\rangle \pm |K_{-n,m}\rangle) - (|K_{n,-m}\rangle \pm |K_{-n,-m}\rangle)]; \\ |A_{\pm n,0}\rangle =& \frac{1}{\sqrt{2}}(|K_{n,0}\rangle \pm |K_{-n,0}\rangle);\ \text{and} \\ |A_{0,\pm m}\rangle =& \frac{1}{\sqrt{2}}(|K_{0,m}\rangle \pm |K_{0,-m}\rangle); \end{aligned} \tag{23}$$

actually achieves the QFI in two special cases of either a purely transversely separated or axially separated source pair, as we show in Ref. [13]. Unlike the pure $\{|K_{nm}\rangle\}$ (K) basis, however, they are able to sense the orientation of the separation vector as well with maximum discrimination allowed by the QFI. But these are not pure phase states, and thus do not have 100% photon throughput, which may be a practical issue in situations of low-light levels as might be true for light scattered by either small or poorly reflecting debris in the space environment. It turns out, however, as we shall see in the next subsection, that the pure-K basis yields CFI that is quite close to the QFI at least for resolving the transverse and axial separations for sub-diffractive separations.

3.3 Numerical Results

We plot in Figs. 1 (a) and (b) the CFIs per photon for the two different measurement schemes discussed in the the previous two subsections. The abscissa on these plots is the actual separation, $\sigma = 2|\boldsymbol{l}_\perp|$ or $\tau = 2l_z$, between the source pair that are laterally or axially separated, respectively. Correspondingly, the CFI and QFI are each a factor of 4 smaller in the two cases compared to the corresponding values for $|\boldsymbol{l}_\perp|, l_z$ discussed earlier.

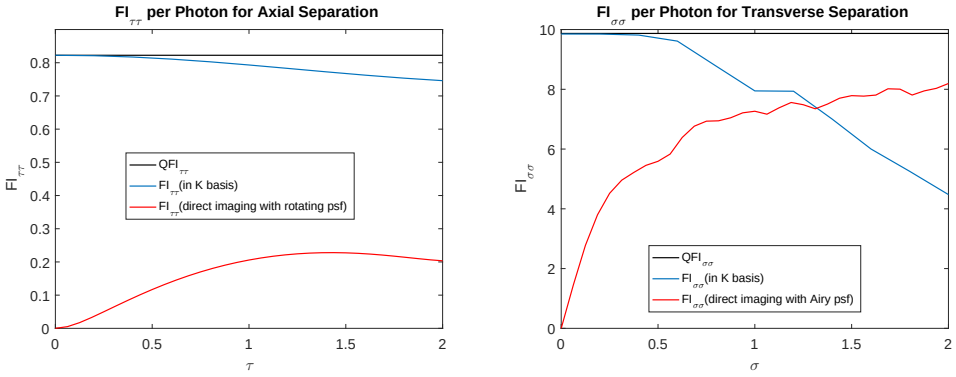

(a) (b)

Figure 1: (a) QFI (black line) and CFI (turquoise for K basis and red for image-based data) for axial separation parameter, $\tau = 2l_z$; (b) Same as (a) except for transverse separation, $\sigma = 2|\boldsymbol{l}_\perp|$.

Note that the CFI for image based data always start at 0 in the limit of vanishing pair separation, as we had noted earlier, but the CFI for projective measurements in the K basis always tend to the QFI in this limit. This implies a scaling law for the minimum photon number, $N_{\min}$, in the regime of highly sub-diffractive separation, needed to estimate such separations scaling as inverse quadratically, $N_{\min} \sim 1/|\boldsymbol{l}_\perp|^2$ and $N_{\min} \sim 1/l_z^2$ in the two cases when using projective measurements in the K basis. This is quite a far cry from the qualitatively more stringent inverse-quartic scaling that, as we noted earlier, image based measurements entail.

From a practical point of view, making projective measurements simultaneously in the full basis is, in general, impossible. We may, however, argue, following the original work of Tsang, *et al.* [10], that only a few such measurements, perhaps even only one, may be needed to approach the QFI in the vanishing separation limit and thus beat the inverse quartic photon budget scaling for image-data-based OSR. We treat in the next section two such protocols, one involving only one and another involving three projective measurements, the latter of which may be performed serially. We call them binary and quarternary spatial demultiplexing, or simply b-SPADE and q-SPADE, respectively, based on the number of probabilities that are considered in each case (two and four, on including the probability of the explicitly unmeasured states). They can be realized by means of either a maximum-likelihood (ML) estimation, which is guaranteed to achieve CFI in the asymptotic limit, or by digitally generated holograms (DGHs) [11] which may be a more sensitive method to achieve nearly CFI-limited performance even at modest photon numbers.

4 SPADE and Realization of QFI by Small Numbers of Projective Measurements

As the original paper [10] showed, it might be possible to approach the QFI in the small-separation limit by performing only a few projective measurements, say M of them that are the most sensitive measurements in that they provide the largest contributions to the CFI. Such measurements, as noted in [11], typically would have among the largest first order derivatives of the probability distribution (PD) w.r.t. the pair separation parameter, say θ_μ, but occurring with only small probabilities, as the contribution of a state, labeled, say, by quantum numbers nm, to the CFI scales as $P_{nm}^{-1}(\partial P_{nm}/\partial\theta_\mu)^2$.

For the single-photon state given by the density operator (5), let us consider making M different projective measurements into a set of M states that we may label as $\{|K_l\rangle|\, l = 1, \ldots, M\}$. This realizes an $(M+1)$-order SPADE, with the $M+1$ probabilities, $P_1, \ldots, P_M, 1-(P_1+\cdots+P_M)$, that add up to 1. The diagonal elements of the CFI for such a SPADE is given by the sum,

$$J_{\mu\mu}^{(M+1)} = \sum_{l=1}^{M} \frac{1}{P_l}\left(\frac{\partial P_l}{\partial\theta_\mu}\right)^2 + \frac{1}{\left(1-\sum_{l=1}^{M} P_l\right)}\left(\sum_{l=1}^{M}\frac{\partial P_l}{\partial\theta_\mu}\right)^2. \tag{24}$$

For $M = 1$ (b-SPADE), this reduces to the simple form,

$$J_{\mu\mu}^{(2)} = \frac{1}{P_1(1-P_1)}\left(\frac{\partial P_1}{\partial\theta_\mu}\right)^2. \tag{25}$$

For b-SPADE, we always choose to project the single-photon state from the two emitters into the state corresponding to a photon emitted by a single source at the origin and imaged through the same imager, namely $|K_{00}\rangle = |K; \mathbf{0}, 0\rangle$, which is the fundamental state of the K basis defined previously.

4.1 Binary SPADE

The projective measurement of the single photon state into the state, $|K_{00}\rangle$, has the probability given by the expectation value, $P_1 = \langle K_{00}|\hat{\rho}|K_{00}\rangle$. In the limit of vanishing pair separation, this is the only state that can be reached by the photon, as all other states, $|K_{nm}\rangle,\ (n,m) \neq (0,0)$, are orthogonal to $|K_{00}\rangle$ and have thus zero probability. However, the ratio (24) that defines the CFI for b-SPADE does not vanish in the limiting sense, as it turns out, and in fact always tends to QFI in this limit. We see this in the two panels of Fig. 2 in which the CFI with respect to the transverse and axial separations are plotted for a number of values of the axial and transverse separations, respectively. We see the well approximated CFI in the b-SPADE protocol when small separations are considered. Note also that the b-SPADE as presented here with the only projective measurement into the axially centered state that is azimuthally invariant cannot sense the transverse orientation of the pair separation vector.

We also note that there are locations along the separation axis in the left panel where the CFI essentially vanishes. Our b-SPADE cannot estimate these separations as the data statistics lose their first-order sensitivity altogether at these specific values of the transverse separation, two of which are shown to occur near σ values of 1.22 and 1.63. We must make additional measurements to eliminate these singular transverse-separation values.

Finally, we note that whenever the axial separation of the source pair is finite, the CFI relative to the estimation of the transverse separation, as in Fig. 2(a), vanishes in the limit of vanishing values of the latter. However, it recovers to values close to the QFI rapidly as the transverse separation becomes non-zero. The same holds when the two separation coordinates switch places, as in Fig. 2(b). This is not well understood.

4.2 Quarternary SPADE

Consider now the projective measurement of the single photon state into three different mutually orthogonal states, namely $|K_{00}\rangle$, and centered but anisotropic sine and cosine states that have the following normalized image-plane

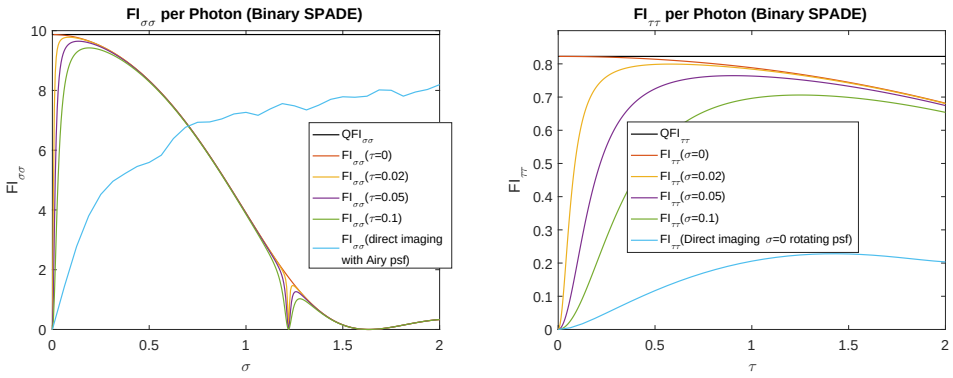

(a) (b)

Figure 2: (a) QFI (black line) and CFI w.r.t. the transverse separation, $\sigma = 2l_\perp$, for a variety of values of the axial separation, as listed, under b-SPADE.(b) Same as (a) except w.r.t. the axial separation, $\tau = 2l_z$, for a variety of values of the transverse separation. Image-data-based CFI, already included in Figs. 1, is also presented on both panels for quick comparison.

coordinate representations:

$$\langle \mathbf{s}|K_c\rangle = \frac{2}{\sqrt{\pi}} \int d^2u\, P(u)\, u\, \cos\phi_u\, \exp\left[-i2\pi \mathbf{u}\cdot\mathbf{s} + i\Psi_0(\mathbf{u})\right];$$
$$\langle \mathbf{s}|K_s\rangle = \frac{2}{\sqrt{\pi}} \int d^2u\, P(u)\, u\, \sin\phi_u\, \exp\left[-i2\pi \mathbf{u}\cdot\mathbf{s} + i\Psi_0(\mathbf{u})\right]. \quad (26)$$

These states provide nontrivial discrimination against the orientation of the transverse separation vector, $\boldsymbol{l}_\perp$ with probabilities of the projection into them varying as $\cos^2\phi_s$ and $\sin^2\phi_s$, respectively, for the orientation being along the ϕ_s direction relative to the x axis.

The next panel of figures (Fig. 3) display our FI calculations for this q-SPADE protocol for estimating the transverse (left panel) and axial (right panel) separations. Three simple observations can be immediately made. First, the CFI curve is elevated compared to the b-SPADE curves we plotted in Fig. 1 at finite but small separations in each panel. This is no surprise since we have added further discrimination not just w.r.t. azimuthal-angle estimation, but also made our overall measurement more sensitive to distance estimation. Second, like in Fig. 2, there are still locations along the transverse-separation axis in the left panel at which the CFI becomes quite small, regardless of the (non-zero) value of the axial separation of the source pair. However, the first of the points, that at 1.22 we had noted in Fig. 2, is now greatly raised because of the additional measurements. Finally, the one undesirable characteristic of CFI that we noted for b-SPADE, namely the vanishing of the CFI with respect to one separation coordinate at its zero value when the other separation coordinate is non-zero, is not observed for q-SPADE when the estimation of the transverse separation coordinate is considered, as in Fig. 2(a). However, that is not true for the estimation of the axial coordinate for which the same undesirable feature is seen in Fig. 2(b).

Finally, in Figs. 4, we plot the CFI for transverse separations of the source pair along the x and y axes (top and bottom panels) for a variety of values of their axial separation and two different values (left and right panels) of the other transverse coordinate, the one that in each figure is not estimated. As we immediately note, the CFI is reduced below the QFI even for vanishing separation of the transverse coordinate being estimated when the non-estimated transverse coordinate is increased in its value from 0. Changing the longitudinal separation, however, has little effect on the CFI curves, except in a close vicinity of the locations at which we observe local minima in the CFI curves.

4.3 Experimental Realization of SPADE

As was noted in Ref. [11], the projective measurements entailed in SPADE may be realized by digital holographic (DH) techniques. If one simulates digitally the interference pattern of a tilted plane wave and the coordinate representation of the desired state, say $|K_1\rangle$, into which the projective measurement is sought and then transfers the pattern to a

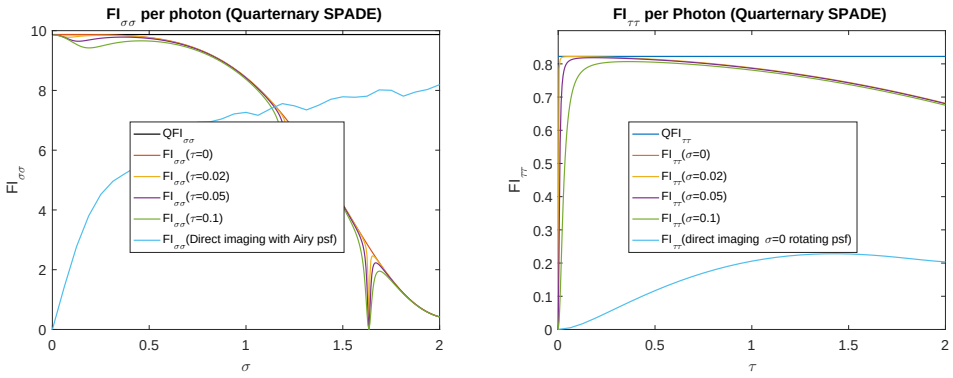

(a) (b)

Figure 3: Same as Figs. 2 except for quarternary SPADE.

phase-amplitude mask, then illuminating the mask with the incoherent-source-pair photon will produce an intensity pattern along the original plane-wave direction that is proportional to the desired absolute-squared sum,

$$\left|\int d^2 s K_1^*(\mathbf{s})\, K(\mathbf{s}; \boldsymbol{l}_\perp, l_z)\right|^2 + \left|\int d^2 s K_1^*(\mathbf{s})\, K(\mathbf{s}; -\boldsymbol{l}_\perp, -l_z)\right|^2 . \tag{27}$$

The intensity pattern along the original reference plane wave can be brought to a focus by a lens, so localized measurements of the requisite probability, proportional to (27), may be made to infer it.

To realize our quarternary SPADE protocol, we will need to repeat this two times with two additional masks corresponding to the two other measurement states and thus take a sequence of three consecutive measurements. If one can assume that the source pair maintains its separation and other emission characteristics during the entire measurement time, then by knowing the total number of photons in each such sequential measurement and recording how many of these photons made it to the focal spot of the original reference wave, one can estimate each requisite probability.

5 Relevance to Astronomical and Space Imaging and Debris Localization Problem

Being steeped in quantum mechanics, the theoretical analysis presented in this paper may seem to belie any relevance of the work to practical problems like astronomical and 3D space-debris localization imaging for which conventional telescopes and rotating-PSF imagers could be employed. But such perceived irrelvance could not be further from the truth. Indeed, the main conclusion of the projective-imaging approach to pair OSR that we have analyzed here is that is eminently practical and applicable to problems of precisely this kind, particularly where photons are scarce and high degrees of OSR are still sought. By reducing the photon budget needed to resolve a pair of closely spaced incoherent point sources to an inverse quadratic law, from its usual inverse quartic form for conventional image-based OSR, one can hope to super-resolve a pair of unresolved faint sources from each other at vastly reduced photon numbers by making projective measurements. Such measurements are easily performed by use of digital holograms and fairly conventional Fourier processing.

The next steps of analysis could focus on the specifics of the 3D space-debris localization problem from the perspective of projective measurements. Basically, by reducing the photon requirements to follow an inverse quadratic law with respect to the spatial localization and resolution errors, all problems, whether of the super-resolution or localization kinds, are reduced, in the projective-measurement protocol, to one of photon localization. It is the accuracy of such photon localization, rather than how closely the sources of such photons are spatially separated, that determines ultimately the ability of an imaging system to image and separate point sources. In fact, from this perspective, the problems of pair OSR and multi-source OSR are essentially no different from the problem of localizing a single source, regardless of any considerations of inter-source distances.

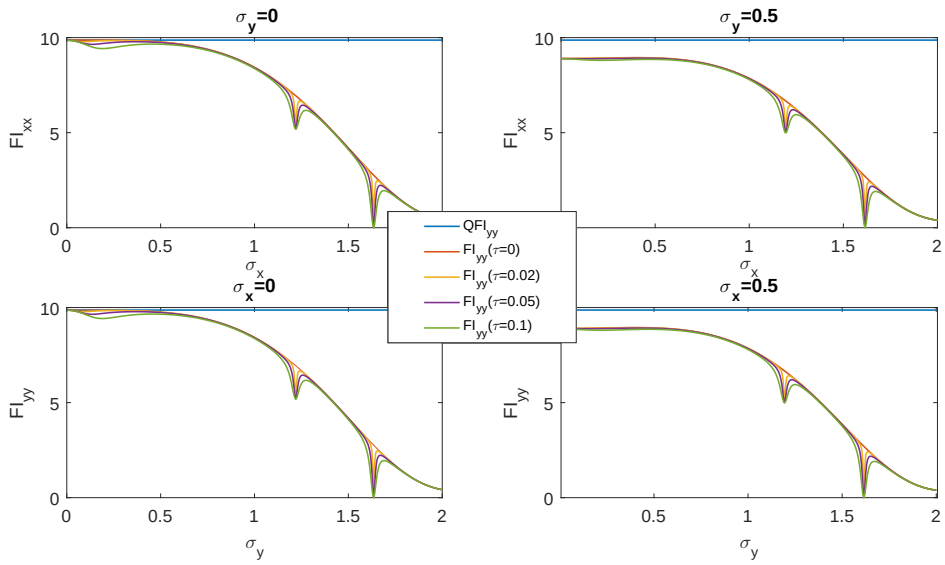

Figure 4: QFI and CFI w.r.t. the transverse x separation, σ_x, for two different y-separations, namely 0 (top left panel) and 0.5 (top right panel); and w.r.t. the transverse y separation, σ_y, for two different x separations, namely 0 (bottom left panel) and 0.5 (bottom right panel). A variety of values of the axial separation, as listed in an insert at the center of the figure, were used for each of the four panels of plots.

Acknowledgments

The work reported here was supported partially by AFOSR grant no. FA9550-15-1-0286.

References

[1] C. Rushforth and R. Harris, "Restoration, resolution, and noise," J. Opt. Soc. Am. **58**, 539–545 (1968).
[2] M. Bertero and C. De Mol, "Superresolution by data inversion," Progress in Optics **XXXVI**, 129–178 (1996).
[3] L. Lucy, "Statistical limits to superresolution," Astron. Astrophys. **261**, pp. 706–710 (1992).
[4] M. Shahram and P. Milanfar, "Imaging below the diffraction limit: a statistical analysis," IEEE Trans. Image Process. **13**, 677–689 (2004).
[5] S. Ram, E. Sally Ward, and R. Ober, "Beyond Rayleigh's criterion: a resolution measure with application to single-molecule microscopy," Proc. Natl. Acad. Sci. USA **103**, 4457–4462 (2006).
[6] S. Prasad, "Asymptotics of Bayesian error probability and 2D pair superresolution," Opt. Express **22**, pp. 16029-16048 (2014).
[7] H. Van Trees, *Detection, Estimation, and Modulation Theory, Part I* (Wiley, 1968), Chap. 2.
[8] S. Kay, *Fundamentals of Statistical Signal Processing: I. Estimation Theory* (Prentice Hall, 1993), Chap. 3.
[9] M. Paris, "Quantum estimation for quantum technology," Int. J. Quant. Inform. **7**, pp. 125137 (2009).
[10] M. Tsang, R. Nair, and X.-M. Lu, "Quantum Theory of Superresolution for Two Incoherent Optical Point Sources," Phys. Rev. X **6**, 031033 (2016).
[11] M. Paur, B. Stoklasa, Z. Hradil, L. Sanchez-Soto, and J. Rehacek, "Achieiving the ultimate optical resolution," Optica **10**, pp. 1144-1147 (2016).
[12] S. Prasad, "Rotating Point Spread Function by Pupil Phase Engineering," Opt. Lett. **38**, pp. 585-587 (2013).
[13] Z. Yu and S. Prasad, "Quantum limited estimation of 3D source-pair separation," in preparation (2017).